# Transport Measurement of Andreev Bound States in a Kondo-Correlated Quantum Dot

Bum-Kyu Kim,[1,2] Ye-Hwan Ahn,[1,3] Ju-Jin Kim,[2] Mahn-Soo Choi,[3] Myung-Ho Bae,[1] Kicheon Kang,[4] Jong Soo Lim,[5] Rosa López,[5,6] and Nam Kim[1]

[1]*Korea Research Institute of Standards and Science, Daejeon 305-340, Republic of Korea*
[2]*Department of Physics, Chonbuk National University, Jeonju 561-756, Republic of Korea*
[3]*Department of Physics, Korea University, Seoul 136-713, Republic of Korea*
[4]*Department of Physics, Chonnam National University, Gwangju 500-757, Republic of Korea*
[5]*Institut de Física Interdisciplinar i de Sistemes Complexos IFISC (CSIC-UIB), E-07122 Palma de Mallorca, Spain*
[6]*Departament de Física, Universitat de les Illes Balears, E-07122 Palma de Mallorca, Spain*

(Received 11 September 2012; published 13 February 2013)

We report nonequilibrium transport measurements of gate-tunable Andreev bound states in a carbon nanotube quantum dot coupled to two superconducting leads. In particular, we observe clear features of two types of Kondo ridges, which can be understood in terms of the interplay between the Kondo effect and superconductivity. In the first type (type I), the coupling is strong and the Kondo effect is dominant. Levels of the Andreev bound states display anticrossing in the middle of the ridge. On the other hand, crossing of the two Andreev bound states is shown in the second type (type II) together with the 0-$\pi$ transition of the Josephson junction. Our scenario is well understood in terms of only a single dimensionless parameter, $k_B T_K^{\min}/\Delta$, where $T_K^{\min}$ and $\Delta$ are the minimum Kondo temperature of a ridge and the superconducting order parameter, respectively. Our observation is consistent with measurements of the critical current, and is supported by numerical renormalization group calculations.

DOI: 10.1103/PhysRevLett.110.076803 PACS numbers: 73.23.−b, 03.65.Yz, 73.63.Kv

In an Andreev reflection process at the interface between a normal metal (or any other nonsuperconducting region) and a superconductor, an electron in the normal region is converted to a Cooper pair necessitating a reflection of a hole. Multiple Andreev reflections (MAR) play a central role in finite-bias transport through a nonsuperconducting region sandwiched by two superconducting leads [1–5]. Contrary to MAR peaks at finite bias, Andreev bound states (ABSs) are formed as a result of coherent superposition of all possible Andreev reflection processes (to the infinite number). So far, ABSs have been observed either in equilibrium across two superconducting electrodes [6], or in a system with only one superconducting lead [7,8]. The interplay of ABSs with the Kondo effect in a quantum dot (QD) coupled to two superconductor leads is an interesting issue, particularly in the context of the 0-$\pi$ transition [9–14]. The "$\pi$ state," exhibiting the reversed sign of the Josephson current of the QD with two superconductor leads, originates from an unpaired electron spin in a strongly interacting QD [9,10]. The usual "0 state" is recovered due to the Kondo screening in the strong coupling limit. Theoretically, it has been shown that this 0-$\pi$ transition is followed by the level crossing of two ABSs [15]. Interestingly, the nature of the ground state is switched between the "0-state" and the "$\pi$-state" at the ABS crossing point. However, simultaneous observation of ABS level crossing and the 0-$\pi$ transition has never been achieved experimentally.

In this Letter, we report a clear signature of a gate-tunable ABS in nonequilibrium transport through a carbon nanotube (CNT) QD asymmetrically coupled to two superconducting leads. In particular, we show that a nonequilibrium transport measurement probes the ABS (which is regarded as an equilibrium property) together with the 0-$\pi$ transition in Josephson critical current ($I_c$) measurement. Further, we find that the interplay between ABSs and the Kondo correlation plays a major role in transport. This leads to the two different prototypes of the Kondo ridges depending on the ratio $k_B T_K^{\min}/\Delta$. $T_K^{\min}$ and $\Delta$ represent the minimum Kondo temperature of the ridge and the superconducting order parameter, respectively. A "type-I" Kondo ridge with a stronger coupling ($k_B T_K^{\min}/\Delta \gtrsim 0.8$) displays an anticrossing of ABSs, where the Josephson junction is always in the "0 state". On the other hand, a "type-II" Kondo ridge with a weaker coupling ($k_B T_K^{\min}/\Delta \lesssim 0.8$) shows a crossing of ABSs, which is directly related to the 0-$\pi$ transition of the Kondo-correlated Josephson junction. Our transport data clearly show two types of Kondo ridge in a single sample. This scenario is confirmed by our measurement of a gate-dependent Josephson critical current $I_c$ along the ridge. In addition, our experimental result is supported by numerical renormalization group (NRG) calculations.

*Experimental setup.*—CNTs are grown by the conventional chemical vapor deposition method on $SiO_2$/Si (500 nm/500 $\mu$m) wafer [16]. A CNT is located by atomic force microscopy. Contact electrodes (10 nm/80 nm Ti/Al bilayer) are subsequently realized by electron-beam lithography and successive electron beam evaporation processes [17]. The Ti layer is used as an adhesion

 

layer between the superconducting Al layer and the CNT. The superconducting transition temperature $T_c$ of the bilayer is about 1.1 K. All measurements are performed at a base temperature below 100 mK in a dilution refrigerator. Two terminal dc measurements are done both in the current and in the voltage bias modes by using a dc voltage-current source (Yokogawa GS200), as shown in Fig. 1(a) [18]. Al superconducting electrodes are switched to normal state by applying an external magnetic field of ~1 kG at the base temperature.

The normal state differential conductance $dI/dV_{sd}$ is plotted in Fig. 1(b), providing a typical even-odd behavior with pronounced Kondo peaks at the zero bias of odd-number ridges. From Fig. 1(b), we extract a charging energy $U \sim 3$ meV and a level separation $\delta E \sim 3$ meV. The Kondo temperature $T_K$, estimated from the half width at half maximum of the Kondo peaks [19], depends on the gate voltage. The minimum Kondo temperature $T_K^{\min}$ in the middle of each Kondo ridge is estimated to be 0.94, 1.6, 2.6, 2.4, and 0.86 K for the Kondo ridges *A*-*E*, respectively. The tunnel coupling $\Gamma$ $(= \Gamma_R + \Gamma_L)$ [with tunnel coupling to the right (left) electrode $\Gamma_R$ $(\Gamma_L)$] is estimated by fitting $T_K$ data to the formula $k_B T_K = (U\Gamma/2)^{1/2} \exp[-\pi(|4\varepsilon^2 - U^2|)/8U\Gamma]$, where $\varepsilon$ is the energy level in the QD tuned by gate voltages [20,21]. The estimated values of the $\Gamma$ range from 0.35 to 0.96 meV for ridges *A*-*E*. The asymmetry ratio $\gamma$ $(= \Gamma_R/\Gamma_L)$ is obtained from the relation $G_{\max} = (2e^2/h)4\Gamma_R\Gamma_L/(\Gamma_R + \Gamma_L)^2$ [22], where $G_{\max}$ is the zero-bias linear conductance obtained in the middle of each Kondo ridge (not shown here) [23]. The estimated $\gamma$ is 2.7, 16, 2.3, 12, and 3.1 for ridges *A*-*E*, respectively. This asymmetry plays an important role in ABS-assisted transport, as we discuss below.

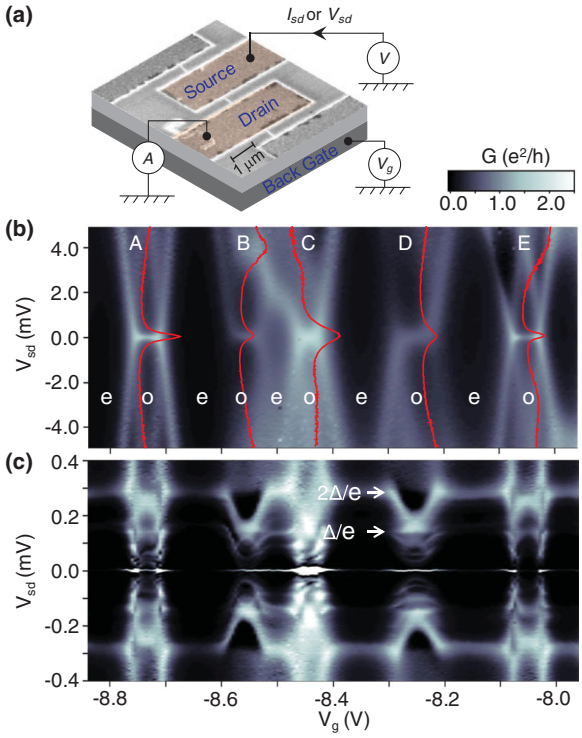


FIG. 1 (color). (a) Schematic of the measurement configuration. Highly doped Si wafer and $SiO_2$ layer are used as a back gate and an insulating barrier, respectively. Channel length of the CNT is designed to be 300 nm. Diameter of the CNT ~1.5 nm is measured by AFM. Differential conductance $dI/dV_{sd}$ plot as a function of $V_{sd}$ and $V_g$ is displayed (b) for normal (with magnetic field $B$ ~1 kG), and (c) for superconducting states at zero field, respectively. The letters e and o denote the even and odd number states, respectively. Bias voltages corresponding to $\Delta/e$ and $2\Delta/e$ (with $\Delta \sim 140$ $\mu$eV) are indicated by arrows in (c). Red curves in (b) correspond to $dI/dV_{sd}$ vs $V_{sd}$ in the middle of the Kondo ridges *A*-*E*.

*Main features of the finite-bias transport.*—Differential conductance with the superconducting leads is displayed in Fig. 1(c). While the even number state shows the gate-independent (elastic) quasiparticle cotunneling ($eV_{sd} = \pm 2\Delta$) [24] together with a weak single Andreev reflection ($eV_{sd} = \pm\Delta$) peaks, the odd-number state displays a rich subgap structure ($|eV_{sd}| < 2\Delta$), which originates from the interplay between the Kondo effect and superconductivity [19]. The most prominent feature is the two different prototypes of the Kondo ridges. This can be seen more clearly in Fig. 2(a), a magnified view of ridges *D* and *E* in Fig. 1(c). Figure 2(a) displays a strong subgap transport. We focus on the main peaks ($V_{sd} = V_{\rm ABS}$) which vary from $|eV_{\rm ABS}| = \Delta$ to $|eV_{\rm ABS}| = 2\Delta$ as a function of the gate voltage (blue dashed lines). Such strong peaks cannot be understood in terms of the perturbative MAR peaks. Notably, this gate-dependent peak in the Kondo ridge evolves into the elastic quasiparticle cotunneling peak at $|eV_{sd}| = 2\Delta$ in the even valley.

We attribute these main peaks to ABS-assisted transport, which is illustrated in Fig. 2(b). In highly asymmetric junctions, ABSs are formed mainly between the QD and a lead with a lower barrier [left lead in Fig. 2(b)]. The other lead with a higher barrier would play the role of a probing ABS. In this picture, the gate-dependent bright peaks at $V_{sd} = V_{\rm ABS}$ result from the alignment of the ABS and the gap edge of the "probe" lead. Together with the fact that the ABS is always formed in a pair with the electron-hole symmetry [15], this gives the following relation between ABS energy ($\varepsilon_a$) and the peak position ($V_{\rm ABS}$):

$$\varepsilon_a = \pm(|eV_{\rm ABS}| - \Delta). \quad (1)$$

The gate-dependent ABS obtained from this relation is plotted in Fig. 2(c). The ABS displays two distinct features depending on the type of the Kondo ridges. A type-I ridge (ridge *D*) with a stronger coupling displays an anticrossing in the middle of the ridge where the Kondo temperature has its minimum value. On the other hand, a type-II ridge (ridge *E*) shows two clear crossing points of the ABS, which is related to the 0-$\pi$ transition. The two different types are determined by the ratio $k_B T_K^{\min}/\Delta$. In the type-I

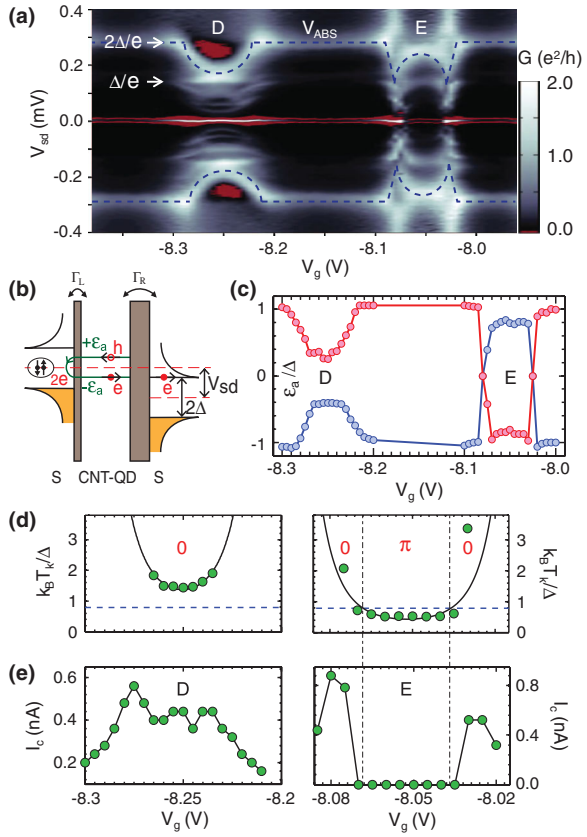


FIG. 2 (color). (a) Differential conductance plot for the two types of the Kondo ridge (magnified view of Fig. 1(c) for ridges $D$ and $E$). Red color represents the region of the negative differential conductance. Blue dashed lines ($V_{\mathrm{ABS}}$) are associated with the ABS-assisted transport (see the text). (b) Schematic diagram of the major transport process forming the Andreev bound states at finite bias. This mechanism is expected to be pronounced in highly asymmetric barriers, where the Andreev bound states are pinned to the lead with a stronger coupling. (c) The ABS level position $\varepsilon_a$ (in units of $\Delta$) obtained from Eq. (1) is plotted as a function of $V_g$. (d) $k_BT_K/\Delta$ vs $V_g$ for ridges $D$ (type-I) and $E$ (type-II), respectively. Filled circles and solid lines correspond to the experimental data and the theoretical fit with the formula $k_BT_K = (U\Gamma/2)^{1/2} \times \exp[-\pi[|4\varepsilon^2 - U^2|]/8U\Gamma]$, and $U/\Delta = 21.4$. The dashed line at $k_BT_K/\Delta = 0.788$ is the theoretically expected '0-$\pi$ transition' line [13]. (e) $I_c$ vs $V_g$ for ridges $D$ and $E$, respectively. Solid lines provide a guide for the eye. $I_c$-$V_g$ curves for ridge $E$ show a sharp drop around the 0-$\pi$ transition point denoted by the two vertical dashed-dotted lines.

ridge, this ratio is always larger than the critical value ($k_BT_K^{\min}/\Delta \simeq 0.8$) [left panel of Fig. 2(d)]. In contrast, the Kondo temperature in the type-II ridge has two transition points corresponding to the 0-$\pi$ transition in the right panel of Fig. 2(d).

*Critical currents.*—Our scenario is further supported by the behavior of the Josephson critical current, $I_c$ [Fig. 2(e)] [25]. A high Josephson current flows due to the Kondo-assisted transmission in the strong coupling ridge (type I), and the system is always in "0 state" [left panel of Fig. 2(e)]. In the type-II ridge, the 0-$\pi$ transition leads to a dramatic change in the behavior of $I_c$ [right panel of Fig. 2(e)]. As the Kondo effect is suppressed in the middle of the ridge, the "$\pi$ state" appears, and it leads to a strong suppression of $I_c$. All these features are consistent with the behavior of the gate-dependent ABS of Fig. 2(c). This behavior of the supercurrent has also been reported in Ref. [21], without delving it into ABS in finite-bias transport.

*Numerical results.*—Our main observation in Fig. 2 is nicely supported by NRG calculation. Figure 3(a) shows the calculated ABS level $\varepsilon_a/\Delta$ as a function of the QD energy level $\varepsilon_d$. It clearly displays two different prototypes, i.e., anticrossing (left) and crossing (right) of the ABS for parameter values of $\Gamma/\Delta = 4.9$ and 3.0, respectively (these values correspond to the experimentally extracted values for ridges $D$ and $E$, respectively). Theoretical values of $I_c$ are determined by the amplitude of the current-phase relation at zero bias voltage. Figure 3(b) shows the QD-level dependence of $I_c$ for the two types of ridge. As in the experimental result of Fig. 2(e), a large Josephson current is assisted by the Kondo effect for the type-I ridge. Suppression of the supercurrent is clearly shown for the type-II ridge at the "$\pi$ state" [right panel of Fig. 3(b)]. This sudden drop of the supercurrent takes place exactly at the 0-$\pi$ transition point. All the features in the calculations match perfectly with the experimental observation in Fig. 2 [26].

*Universality of ABS-assisted transport.*—We note that the gate-independent peaks for the even number state at

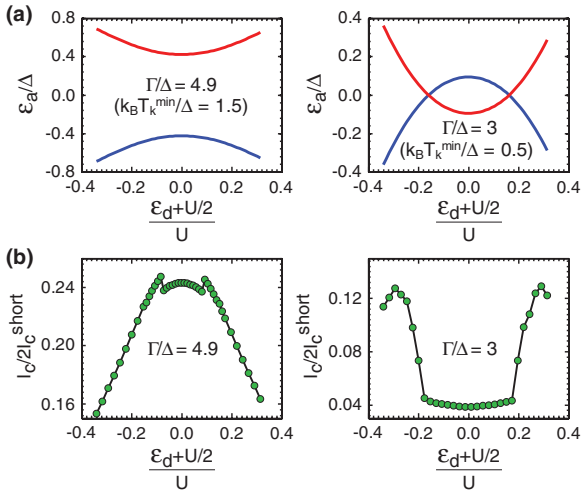


FIG. 3 (color). NRG results for the two types of Kondo ridge: (a) ABS level position $\varepsilon_a$ (in units of $\Delta$) and (b) the Josephson critical current $I_c$ as a function of the QD energy level $\varepsilon_d$. Both in (a) and (b), coupling constants $\Gamma/\Delta = 4.9$ (left panels) and $\Gamma/\Delta = 3.0$ (right panels) are used, which correspond to the experimental values of ridges $D$ (type-I) and $E$ (type-II), respectively. Experimentally extracted value of $U/\Delta = 21.4$ is used in both cases. $k_BT_K^{\min}/\Delta$ are 1.5 and 0.5 for ridges $D$ and $E$, respectively.

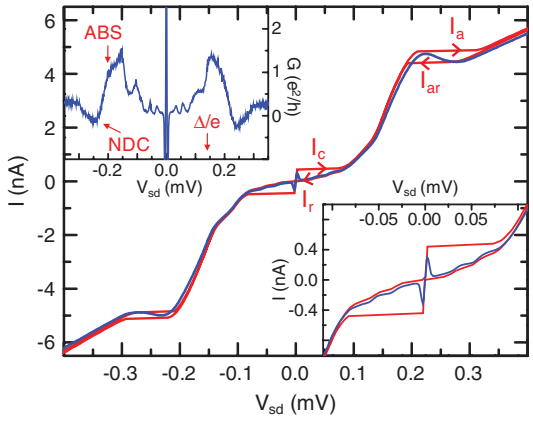


FIG. 4 (color). $I$-$V_{sd}$ curves measured in current bias (red line), and voltage bias (blue line) modes, respectively, in the middle of Kondo ridge $D$ ($V_g = -8.255$ V). Two switching currents, $I_c$ and $I_a$, appear at zero voltage and at $V \approx 0.2$ mV, respectively. The slope of the supercurrent branch is mainly due to the resistance of low pass filters ($\sim 4$ kΩ). Upper-left inset: differential conductance $G = dI/dV_{sd}$ vs $V_{sd}$ in voltage bias mode. Lower-right inset: magnified view of the $I$-$V$ curve around zero bias.

$eV_{sd} = \pm 2\Delta$ can also be understood within our framework of ABS-assisted transport. Of course, these peaks can be identified as the elastic cotunneling of quasiparticles [24]. On the other hand, ABSs are pinned to $\varepsilon_a = \pm\Delta$ in the off-resonance limit of the even valley. In this case, ABS-assisted transport also provides peaks at $eV_{sd} = \pm 2\Delta$, according to Eq. (1). That is, ABS peaks evolve into the quasiparticle cotunneling peaks in the off-resonance limit. Therefore, the main features of transport can be understood in a very universal way, ranging from the Coulomb blockade (off-resonance), the intermediate coupling ($\pi$ state), to the strong Kondo limit (0 state).

*Negative dynamic conductance and fine structures.*—Another evidence of ABS-assisted transport is shown in the negative dynamic conductance (NDC) region in the voltage bias mode (blue line in Fig. 4). It can be more clearly seen in $dI/dV_{sd}$ [upper-left inset of Fig. 4 and the red-colored region in Fig. 2(a)]. A hysteretic switching current above $I_c$ is found in a current bias at $I = I_a$ (forward) or $I = I_{ar}$ (backward) depending on the direction of the current sweep. NDC and the hysteretic switching current can be understood as a general feature when a Cooper pair tunnels through a resonant state in a QD [27–29]. For highly asymmetric barriers [as illustrated in Fig. 2(b)], resonant ABSs formed with the lower barrier lead can be probed by the "probe" lead. However, as tunneling barriers become more symmetric, ABS levels are not well defined at finite bias and NDC is expected to disappear. Actually, NDC and the hysteretic switching current at $I = I_a$ and $I = I_{ar}$ are observed only for ridges $B$ and $D$ whose asymmetry ratio is very large ($\gamma = 16$ and $\gamma = 12$ for ridges $B$ and $D$, respectively). When one of the two tunneling barriers is significantly higher than the other, our measurement configuration is equivalent to scanning tunneling microscope measurement with a superconducting tip. Thus, the dynamic conductance density plots for ridges $B$ and $D$ reflect the density of states in the CNT-QD as shown in Refs. [6–8].

Finally, we briefly discuss the fine structures in the differential conductance at lower voltage, $|eV_{sd}| < \Delta$ in Figs. 1(c) and 2(a). Although a quantitative analysis for this is beyond our scope, we notice that the smaller peaks at $|eV_{sd}| < \Delta$ greatly resemble the gate dependence of the main peaks at $V_{sd} = V_{\mathrm{ABS}}$ for both types of Kondo ridge. Therefore, we speculate that these small peaks originate from the combination of ABSs (mainly formed with the lower barrier contact) and single or multiple Andreev reflections (with a higher barrier contact).

*Conclusion.*—In conclusion, gate tunable ABSs are reported in $I$-$V$ measurement configuration in an Al-CNT-Al Josephson junction. The observed differential conductance shows the two distinct types of Kondo ridges associated with ABSs. An ABS displays crossing (anticrossing) behavior, which is the main characteristic of the 0-$\pi$ transition (0 junction) tuned by a gate voltage applied to the QD. This feature is also consistent with a measurement of the gate-dependent critical current, and is confirmed by a numerical renormalization group calculation.

We acknowledge valuable discussions with Yong-Joo Doh and thank Hyun-Ho Noh and Woon Song for assistance in measurement. This work was supported by the National Research Foundation of Korea (NRF) (Grants No. 2009-0084606, No. 2012R1A1A2003957, No. 2010-0025880, No. 2011-0012494, and No. 2011-0015895), and by the Korea Research Institute of Standards and Science. R. L and J. S. L were supported by MINECO Grants No. FIS2008-00781, No. FIS2011-23526, and No. CSD2007-00042 (CPAN).

[1] M. Jung, H. Noh, Y.-J. Doh, W. Song, Y. Chong, M.-S. Choi, Y. Yoo, K. Seo, N. Kim, B.-C. Woo, B. Kim, and J. Kim, ACS Nano **5**, 2271 (2011).
[2] H. Takayanagi and T. Akazaki, Phys. Rev. B **52**, R8633 (1995).
[3] X. Du, I. Skachko, and E. Y. Andrei, Phys. Rev. B **77**, 184507 (2008).
[4] M. R. Buitelaar, W. Belzig, T. Nussbaumer, B. Babic, C. Bruder, and C. Schonenberger, Phys. Rev. Lett. **91**, 057005 (2003).
[5] J. Xiang, A. Vidan, M. Tinkham, R. M. Westervelt, and C. M. Lieber, Nat. Nanotechnol. **1**, 208 (2006).
[6] J.-D. Pillet, C. H. L. Quay, P. Morfin, C. Bena, A. L. Yeyati, and P. Joyez, Nat. Phys. **6**, 965 (2010).
[7] T. Dirks, T. L. Hughes, S. Lal, B. Uchoa, Y.-F. Chen, C. Chialvo, P. M. Goldbart, and N. Mason, Nat. Phys. **7**, 386 (2011).

[8] R. S. Deacon, Y. Tanaka, A. Oiwa, R. Sakano, K. Yoshida, K. Shibata, K. Hirakawa, and S. Tarucha, Phys. Rev. Lett. **104**, 076805 (2010).
[9] L. I. Glazman and K. A. Matveev, Pis'ma Zh. Tekh. Fiz. **49**, 570 (1988) [JETP Lett. **49**, 659 (1989)].
[10] B. I. Spivak and S. A. Kivelson, Phys. Rev. B **43**, 3740 (1991).
[11] M.-S. Choi, M. Lee, K. Kang, and W. Belzig, Phys. Rev. B **70**, 020502 (2004).
[12] F. Siano and R. Egger, Phys. Rev. Lett. **93**, 047002 (2004).
[13] G. Sellier, T. Kopp, J. Kroha, and Y. S. Barash, Phys. Rev. B **72**, 174502 (2005).
[14] J. A. van Dam, Y. V. Nazarov, E. P. A. M. Bakkers, S. De Franceschi, and L. P. Kouwenhoven, Nature (London) **442**, 667 (2006); J.-P. Cleuziou, W. Wernsdorfer, V. Bouchiat, T. Ondarcuhu, and M. Monthioux, Nat. Nanotechnol. **1**, 53 (2006); H. I. Jørgensen, T. Novotny, K. Grove-Rasmussen, K. Flensberg, and P. E. Lindelof, Nano Lett. **7**, 2441 (2007).
[15] J. S. Lim and M.-S. Choi, J. Phys. Condens. Matter **20**, 415225 (2008); J. Bauer, A. Oguri, and A. C. Hewson, J. Phys. Condens. Matter **19**, 486211 (2007).
[16] J. Kong, H. T. Soh, A. M. Casse, C. F. Quate, and H. Dai, Nature (London) **395**, 878 (1998).
[17] B.-K. Kim, J.-J. Kim, M. Seo, Y. Chung, B.-C. Woo, J. Kim, W. Song, and N. Kim, Appl. Phys. Lett. **97**, 262110 (2010).
[18] In order to suppress high frequency noise from heating sample, low-pass RC filters with a cut-off frequency of $\sim$10 kHz are mounted on the sample chip. The line resistance including filters in a two-terminal configuration is measured to be $\sim$4 k$\Omega$. Low pass filters are essential to observe the switching current in small magnitude.
[19] M. R. Buitelaar, T. Nussbaumer, and C. Schonenberger, Phys. Rev. Lett. **89**, 256801 (2002).
[20] A. M. Tsvelick and P. B. Wiegmann, Adv. Phys. **32**, 453 (1983); F. D. M. Haldane, Phys. Rev. Lett. **40**, 416 (1978).
[21] A. Eichler, R. Deblock, M. Weiss, C. Karrasch, V. Meden, C. Schonenberger, and H. Bouchiat, Phys. Rev. B **79**, 161407 (2009).
[22] G. L. I. Glazman and M. E. Raikh, Pis'ma Zh. Eksp. Teor. Fiz. **47**, 378 (1988) [JETP Lett. **47**, 452 (1988)]; T. K. Ng and P. A. Lee, Phys. Rev. Lett. **61**, 1768 (1988).
[23] This is possible because every Kondo ridge is almost in the unitary limit ($T \ll T_K$) in our base temperature.
[24] K. Grove-Rasmussen, H. I. Jorgensen, B. M. Andersen, J. Paaske, T. S. Jespersen, J. Nygård, K. Flensberg, and P. E. Lindelof, Phys. Rev. B **79**, 134518 (2009).
[25] $I_c$ is measured from the switching current in the $I$-$V$ curve as shown in Fig. 4.
[26] Symmetric coupling is considered in our calculation. Note that the asymmetry $\gamma$ does not modify the position of the ABS, and gives only a gate-independent reduction of $I_c$.
[27] I. P. Nevirkovets, S. E. Shafranjuk, O. Chernyashevskyy, and J. B. Ketterson, Phys. Rev. Lett. **98**, 127002 (2007).
[28] B. M. Andersen, K. Flensberg, V. Koerting, and J. Paaske, Phys. Rev. Lett. **107**, 256802 (2011).
[29] A. L. Yeyati, J. C. Cuevas, A. Lopez-Davalos, and A. Martin-Rodero, Phys. Rev. B **55**, R6137 (1997).